

# Bioinspired polyimide film with fire retardant and gas barrier properties by gravity-induced deposition of montmorillonite

Qiao-Xi Yu<sup>1</sup>, Run-Xin Bei<sup>1</sup>, Jia-Hui Liu<sup>1</sup>, Yan-Wei He<sup>1</sup>, Siwei Liu<sup>1</sup>, Zhenguo Chi<sup>1</sup>, Jia-Rui Xu<sup>1</sup>, and Yi Zhang<sup>1</sup>

<sup>1</sup>Sun Yat-Sen University

May 26, 2023

## Abstract

Flame retardants play a crucial role in improving the flame retardant properties of polymer materials. In recent years, environmental problems caused by flame retardants have attracted widespread attention. It is urgent to use green and effective methods to prepare flame retardant polymers. Bioinspired nanocomposites with layered structures seem to provide an effective idea, but in general, the hydrophilic properties of their raw materials limit their applications in certain fields. Here, we prepared biomimetic composites with a layered “brick-and-mortar” structure by gravity-induced deposition using polyimide as the polymer matrix and montmorillonite (MMT) as the filler. The well-arranged structures of the composite material could isolate oxygen and prevent combustible gases from escaping. The gas barrier performance has been greatly improved, in which the water vapor transmission rate (WVTR) and the oxygen transmission rate (OTR) decreased by 99.18% and three orders of magnitude, respectively. The flame retardant performance has also been improved, and its limiting oxygen index can reach 67.9%. More importantly, the polyimide matrix can be converted to water-insoluble by thermal imidization of water-soluble poly (amic acid) salt precursors, which endows the composites with low hygroscopicity. Such coating containing MMT can protect against polyurethane (PU) foam from fire. During the conical calorimetric test, the coated sample self-extinguished, and the peak heat release rate, total heat release, total smoke production is significantly decreased by 53.39%, 40.69%, and 53.03%, respectively. Taking advantage of these properties, this work utilizes a facile method to prepare biomimetic composites with low moisture absorption, excellent gas barrier properties, and flame retardancy, which have great application potential.

## 1. Introduction

Polymer materials are widely used in all walks of life nowadays owing to their excellent comprehensive properties, mainly composed of compounds formed by carbon and hydrogen. Therefore, they are prone to fire when exposed to a heat source continuously. Fire hazards caused by combustible polymers have become a serious threat to human life and health and may cause economic losses.<sup>[1]</sup> To improve the flame retardancy of polymer, several commonly used flame retardants are added to the polymer matrix, such as halogenated flame retardants,<sup>[2]</sup> and phosphorus-based flame retardants,<sup>[3]</sup> inorganic flame retardants.<sup>[4]</sup> Although effective, these methods have some obvious shortcomings or deficiencies. Polymers containing halogenated flame retardants will release heavy smoke and corrosive gases (like HBr) during the combustion process, which will bring secondary disasters to people’s life and pollute the environment.<sup>[5, 6]</sup> The use of halogen-free flame retardants can reduce the amount of smoke to a certain extent, but its applicability is not as good as that of halogen-based flame retardants, which will increase the processing difficulty.<sup>[7]</sup> In addition, although inorganic flame retardants such as aluminum hydroxide have the effects of smoke suppression and low toxicity, their flame retardant efficiency is low, and more additives are needed to achieve the desired requirement of flame retardant performance.<sup>[8]</sup> Consequently, a safe, effective, and environmentally friendly strategy for the preparation of polymers with good flame retardant properties is essential and has great potential for application.

Instead of conventional flame retardants, polymer nanocomposites can also be prepared to enhance flame retardancy. Commonly used are layered silicate,<sup>[9]</sup> graphene and its derivatives,<sup>[10]</sup> boron nitride<sup>[11]</sup> and so on. The flame retardant mechanism of nanocomposites is the barrier effect formed by nanomaterials, which not only blocks the diffusion of combustible small molecules produced by the thermal degradation of internal polymer chains to the combustion interface, but also delays the transfer of external oxygen to the combustion interior.<sup>[12]</sup> Unfortunately, small amounts of nanomaterials seem unlikely to form promising barrier effects.<sup>[12]</sup> Therefore, an appropriate amount of nanomaterials must be added to acquire a sufficient barrier effect. However, as the content of nanomaterials increases, the interface between organic and inorganic is un-neglected, and the fillers tend to aggregate and reduce uniformity. Consequently, the flame retardant performance cannot be improved effectively.

One such complex is found in natural materials, nacre, mainly consisting of extremely thin organic matter separated by orderly lamellar calcium carbonate.<sup>[13]</sup> Its hierarchical structure and excellent mechanical properties have attracted extensive attention.<sup>[14, 15]</sup> At present, a variety of preparation methods have been developed, hoping to obtain composite materials with excellent properties by artificially simulating the nacre structure, such as gravity-induced deposition,<sup>[16]</sup> layer-by-layer deposition,<sup>[17]</sup> freeze casting,<sup>[18]</sup> electrophoretic deposition,<sup>[19]</sup> etc. Typically, hydrophilic or water-soluble polymers, such as polyvinyl alcohol (PVA),<sup>[20]</sup> polyacrylic acid (PAA),<sup>[21]</sup> polyethyleneimine (PEI),<sup>[22]</sup> cellulose,<sup>[23]</sup> etc., are used to prepare nacre-like composites, to increase the interfacial compatibility with nano inorganic materials. Apart from the mechanical properties, several other useful functions have been developed, such as a separator for battery,<sup>[24]</sup> thermally conductive film,<sup>[25]</sup> sensor,<sup>[26]</sup> energy storage,<sup>[27]</sup> and so on. Based on the defect-dominated diffusion model first proposed by Prins and Hermans,<sup>[28]</sup> the addition of inorganic flake materials to polymers can effectively prolong the gas diffusion path in the material, thereby significantly improving its barrier properties. Isolate external oxygen to prevent it from entering into the material and avoiding the escape of internal pyrolytic gas can effectively improve the flame retardancy of the material, which shows that bioinspired nacre-like composite will have excellent flame retardant performance.<sup>[29]</sup> The raw materials that artificial bioinspired nacre-like composite is prone to swelling or even dissolution in water. So, when this kind of material is applied to the exterior wall, it is quite easy to be damaged in rainwater, lose its fire effect, and cause economic losses, limiting its scope of application.

Herein, to solve the above problems, we used polyimide (PI) as polymer matrix and montmorillonite (MMT) as lamellar inorganic nanomaterials and prepared water-insoluble bioinspired nacre-like composites with good fire retardancy. PI is a kind of polymer containing imide rings in the main chain<sup>[30]</sup> which has fabulous comprehensive properties, including high chemical stability, thermal stability, and high mechanical properties.<sup>[31, 32]</sup> Particularly, the water insoluble PI can be transformed from the water-soluble precursor poly (amic acid) salt (PAAS) by thermal imidization. Using this transformation, it is possible to make nacre-like composites that are not insoluble or swellable by water. By selecting the PI monomer containing polar groups, PAAS can form a strong interaction with the abundant hydroxyl groups on the MMT surface, elegantly resolving the interfacial problem between them, resulting in homogeneous composites. The MMT sheets attached to the PAAS will gradually sink and accumulate in an orderly manner due to the influence of gravity. Finally, by increasing the temperature to volatilize the solvents and complete thermal imidization, while preserving the ordered structure, the bioinspired polyimide composite was realized. Benefiting from the well-ordered layered structure, the composite shows excellent gas barrier properties, followed by the improvement of its flame retardancy, which is reflected in a significant increase in the limiting oxygen index (LOI). Besides, the composite framework is retained after combustion, which plays a role in delaying the spread of the fire. Surprisingly, even if the PAAS is used as a polymer matrix, composite coating with MMT's still has good flame retardant properties. When PAAS is coated on PU foam, it gives flammable PU foam self-extinguishing performance, and the flame retardant and smoke suppression performance are significantly improved. This is a meaningful discovery. Through structural design, PAAS can be quantitatively imidized at 150°C.<sup>[33]</sup> When PAAS/MMT is coated on some 150 °C resistant foam, it can be converted into PI/MMT coating after quantitative imidization to obtain higher flame retardancy. Moreover, even PAAS/MMT coating can effectively improve the flame retardancy. To sum up, this work will further broaden the application

of bioinspired nacre-like materials in the field of fire protection.

## 2. Materials and methods

### 2.1 Materials

MMT powder (the model is PGN sodium-based MMT) was purchased from Nanocor Inc., America. Its color is dark white, with an average particle size of 5  $\mu\text{m}$ , and its cation exchange capacity (CEC) is  $120\pm 1.2$  meq/100g. 4,4'-Diaminobenzanilide (DABA) and 4,4'-biphtalic anhydride (BPDA) were purchased from J&K Scientific Ltd., China. N, N-dimethyl acetamide (DMAc, water[?]50 ppm), triethylamine (TEA, 99.5%), (3-aminopropyl) triethoxysilane (KH550, 99%), and sodium hydroxide (NaOH, 97%) were supplied by Energy Chemical Co., Ltd., China. Polyvinyl alcohol (PVA, DP [?] 1750+50) was purchased from Sinopharm Chemical Reagent Co., Ltd., China. Carboxymethyl cellulose (CMC, M.W. = 700000) was purchased from Aladdin Biochemical Technology Co., Ltd., China. PI substrates, made by DABA and BPDA were obtained from Wu Xi Shun Xuan New Materials Co., Ltd., China, and named DABPPI. PU foam with a density of 30  $\text{kg}/\text{m}^3$  was purchased from Langfang PU products factory, China. DABA and BPDA were dried in a vacuum oven at 80°C and 150 °C for 8 h before use, respectively. Other chemicals were used as received.

### 2.2 Materials synthesis

*Preparation of MMT nanosheets.* Put 6.0 g MMT and 500 mL deionized water in a beaker and sonicate for 1 h. After that, a yellow turbidity dispersion was obtained. Separate the precipitation with a centrifuge (9000 rpm, 5 min) and collect the transparent solution MMT nanosheet colloid. Finally, the colloid was concentrated by a rotary evaporator at a concentration of 3.2 wt%.

*Preparation of PAAS solution.* First, the PAA solution was obtained by condensation polymerization of BPDA and DABA (molar ratio of 100:99.5) in DMAc (10 wt% solid content) at 5 °C for 12 h. KH550 was then added and stirred for 3 h (KH550: BPDA was 0.01:1). Last, the PAAS solution was prepared by adding TEA (2.0 mol equivalent to BPDA) to the mixture at room temperature and stirring for 4 h.

*Surface treatment of PI substrate.* The method was to cover one side of the DABPPI with 25 wt% NaOH solution for 25 min and then wash it thoroughly and dry it.

*Preparation of the bioinspired polyimide composite film.* A certain amount of MMT colloid was put into a three-neck flask and diluted to 2 wt% with deionized water. Subsequently, PAAS solution was added slowly with gentle agitation (the mass ratio of MMT to PAAS was 1:1). After continuous stirring for 4 h, uniform glue was obtained. The surface-treated PI was sandwiched on the flange ring, and the composite glue (20 mL) was poured onto the PI. The flange ring was placed in an oven and set the heating program to 50 /4 h, 100 /1 h, 150 /1 h, and 220 /1 h. Finally, the bioinspired polyimide composite film was gained and named MMT-PI.

*Preparation of the bioinspired MMT film, MMT-PVA, and MMT-CMC.* The specific preparation steps can be seen in **Supporting Information** .

*Preparation of the coated PU foam.* The PU foam was cut into 10 cmx10 cmx1 cm and then dipped in the MMT-PAAS solution for 10 min. The coated PU foam was placed in an oven and set the heating program to 50 /4 h, 80 /1 h. The coated PU foam was named MMT/PAAS-PU.

### 2.3 Characterization

Fourier transform infrared spectroscopic (FTIR) spectra were obtained by Nexus 670 (Thermo Nicolet, America). The data was collected in attenuated total reflection (ATR) mode with the wavenumber range from 400  $\text{cm}^{-1}$  to 4000  $\text{cm}^{-1}$ . XRD spectra were recorded on Rigaku SmartLab diffractometer with the Cu  $K\alpha$  at the voltage of 40 kV and current of 30 mA over the  $2\theta$  angular range of 2 °~30 ° at the scanning speed of 10 °/min. SEM image was processed on S-4800 (Hitachi, Japan) at an accelerating voltage of 10 kV. Oxygen transmission rate (OTR) was conducted on G2/132 (Labthink, China) based on the differential pressure method. Water vapor transmission rate (WVTR) was determined using W3/330 (Labthink, China) with a

sample test area of  $5 \text{ cm}^2$  at  $37.8^\circ\text{C}$  and  $77.0 \text{ \%RH}$  ( $\pm 1 \text{ \%RH}$ ). The limiting oxygen index (LOI) values were collected by the YZS-75A oxygen index meter (Bei Guang Jing Yi, China) according to GB/T 2406.1-2008. MMT-PI film was fixed 2 cm above the heat source (alcohol lamp flame) and the pseudocolor thermal imager was set at a specific distance for fire-resistance measurement. The thermal infrared imager VH-780 (Infra Tec, Germany) was used to capture pseudocolor thermal images during the 90 s video recording. The test method for water absorption is as follows. The MMT film, MMT-PI, MMT-PVA, and MMT-CMC were completely immersed in deionized water and placed under room temperature and pressure for 3 days. The films were then taken out, and water adhering to the surface of the films was quickly wiped off and weighed immediately. The water absorption rate (WA%) was calculated according to **Eq. 1**.

**Eq. 1**

In **Eq. 1**,  $W_0$  and  $W_t$  are the weight of the film before and after water absorption, respectively.

### 3. Results and discussion

The fabrication process of the composite film is illustrated in **Fig. 1**. First, MMT colloid was obtained after sonication of MMT in water,<sup>[34]</sup> then mixed with PAAS solution. The resulting glue has a brown color, and no precipitation is generated because of the interaction between them, especially the interaction of hydrogen bond. Finally, the glue was poured onto the PI film fixed by the flange ring and put into the temperature-controlled oven. At lower temperature, MMT nanosheets adhered to PAAS gradually precipitated to the bottom under the action of gravity (because of the large aspect ratio of MMT) and were well arranged in a “flat lay” manner. thermal imidization was completed to obtain the final composite film.

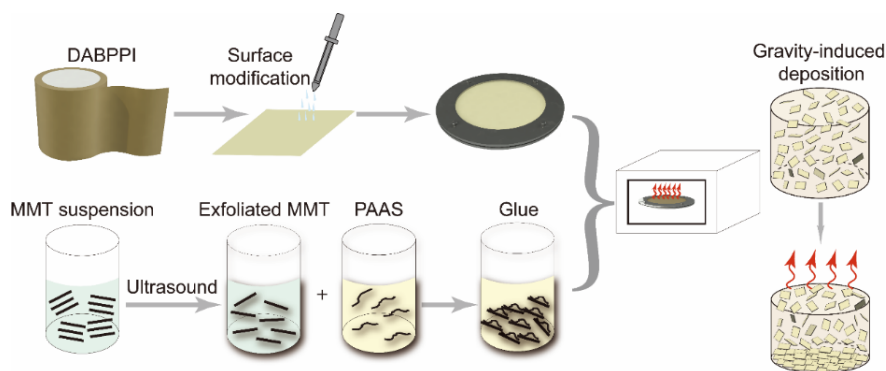


**FIGURE 1** Fabrication process of the MMT-PI composite film.

The monolayer MMT was obtained in the first step, and the MMT colloid was yellow and transparent without precipitation, which shows that the MMT was completely stripped. Moreover, the TEM image shows that the size of the peeled MMT nanosheet was about  $5 \mu\text{m}$  (**Fig. S1** in Supporting Information), which has a reported thickness of about  $1 \text{ nm}$ ,<sup>[35]</sup> and thus its aspect ratio of it was 5000. MMT colloid showed the Tyndall effect (**Fig. S1** in Supporting Information), which proved that fully stripped MMT nanosheets were successfully obtained after high-power ultrasonic treatment.

Afterward, MMT colloid was mixed with a solution of PAAS. The mixture was temperature-programmed to obtain MMT-PI nacre-like composites by gravity-induced deposition. **Fig.2a** is the FTIR spectra of MMT, DABPPI, and MMT-PI. The FTIR of MMT has three characteristic peaks. Among them, the peaks at  $3631 \text{ cm}^{-1}$  and  $3438 \text{ cm}^{-1}$  are assigned to the  $-\text{OH}$  vibration on the surface of MMT, and the hydrogen bonding interaction between MMT and water molecules, respectively. And the spectrum displayed vibration bands at  $1044 \text{ cm}^{-1}$  for Si-O stretching. By observing the results of DABPPI and MMT-PI, the characteristic absorption peaks of the imide ring both appeared around  $1771 \text{ cm}^{-1}$  ( $\text{C}=\text{O}$  stretching vibration) and around  $1370 \text{ cm}^{-1}$  ( $\text{C}-\text{N}$  stretching vibration).<sup>[36, 37]</sup> Due to the existence of DABA, both DABPPI and MMT-PI

have characteristic peaks at  $1642\text{ cm}^{-1}$  (“Amide I”) and  $1513\text{ cm}^{-1}$  (“Amide II”).<sup>[38]</sup> For MMT-PI, there are also absorption peaks at  $3623\text{ cm}^{-1}$  and  $3351\text{ cm}^{-1}$ , which are caused by the hydrogen bonding interaction between MMT and PI, respectively. Furthermore, the red shift of the peak caused by Si-O to  $1013\text{ cm}^{-1}$  also proves the occurrence of hydrogen bonding interactions between them. All the above results indicated that due to the use of diamine DABA with an amide bond, the obtained PI could form strong interactions with the hydroxyl groups on the surface and sides of the MMT, thus facilitating the good dispersion of MMT in the PI matrix.

To explore the aggregate structure of the composite film, XRD was used, and the results are shown in **Fig. 2b**. No obvious diffraction peak was found for DABPPI, so it could be considered an amorphous polymer. For pristine MMT, the results are similar to those reported work,<sup>[39]</sup> the diffraction peak of the (001) plane appears at  $2\theta$  of  $7.2^\circ$ , and the corresponding  $d$  spacing is 1.23 nm. The XRD pattern of MMT-PI shows distinct differences compared to MMT. The peak of the (001) plane was shifted to  $6.7^\circ$  ( $d$  spacing is 2.60 nm), which indirectly demonstrated the fact that the MMT was successfully exfoliated. Moreover, the increment of interlayer spacing between MMT slices may be due to the adhesion of PI chains to MMT. Meanwhile, its full width at half maxima (FWHM) narrows with the increase of its peak intensity, implying the existence of a strongly ordered laminated structure in the MMT-PI.

The ordered layered structure of MMT-PI can be further proved by the SEM. The MMT sheets presented the lay-flat arrangement with few defects due to uneven arrangements or aggregation (**Fig.2c**). In MMT-PI composites, MMT sheets act as “brick” and PI chains act as “mortar”, together forming a so-called biomimetic nacre-like “brick-and-mortar” layered structure. MMT and PI are uniformly distributed, and they show no phase separation (as can be seen from **Fig. S2 a, b**, Supporting Information). The surface SEM results (**Fig.2d**) show that there are no visible defects, and its surface uniformly covers MMT and PI. Similarly, the MMT and PI distribution is homogeneous and has no phase separation (**Fig. S2 c, d** in Supporting Information).

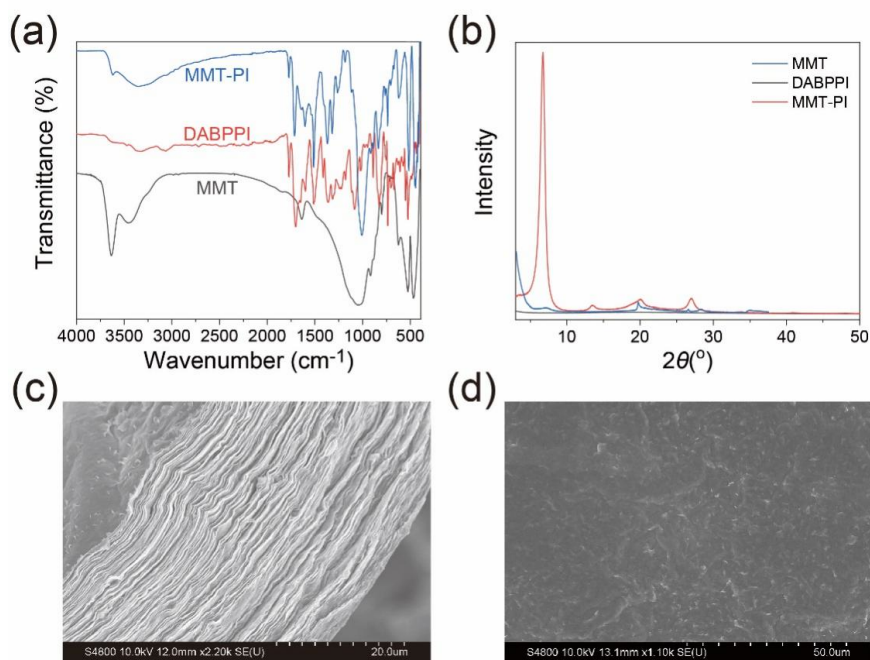


**FIGURE 2** The FTIR spectra of MMT, DABPPI, and MMT-PI (a). The XRD spectra of MMT, DABPPI, and MMT-PI (b). The cross-section (c) and surface (d) SEM images of MMT-PI.

Layered silicate, such as MMT, is reported to be impermeable to gas molecules,<sup>[40]</sup> which makes gas molecules

difficult to penetrate because of its perfect crystal structure. Therefore, the addition of MMT to PI would create a physical obstacle to the diffusion of gas molecules in the composite. From the above SEM results, it could be inferred that it would be very difficult for gas to pass through the composite material with such a “brick-and-mortar” layered structure, which may greatly improve the gas barrier performance of the MMT-PI composite film.

The results of the gas barrier properties of DABPPI and MMT-PI are shown in **Table 1**. Surprisingly, the WVTR of MMT-PI was significantly decreased. The value of WVTR decreased from 2.25 g/m<sup>2</sup>/day for DABPPI to 0.0185 g/m<sup>2</sup>/day for MMT-PI, a decrease of 99.18%. The results of previous studies have shown that the improvement in water vapor barrier properties of nacre-like composites is not very significant due to the hydrophilicity of the raw materials used. This concern is ameliorated by using PI as “mortar”. DABPPI is a kind of water-insoluble PI with relatively low water absorption. Combined with the dense lamellar structure, the diffusion of water molecules can be well hampered, thereby improving the water vapor barrier performance. The nacre-like structure has exceptional barrier properties for non-condensed, non-polar gases, like oxygen, which has also been confirmed by early studies.<sup>[41, 42]</sup> In this study, the oxygen permeability of MMT-PI was decreased conspicuously. Specifically, the DABPPI showed an OTR of 1944.69 cm<sup>3</sup>/m<sup>2</sup>/day/0.1MPa. While with the addition of 50% MMT, the OTR decreased to 7.98 cm<sup>3</sup>/m<sup>2</sup>/day/0.1MPa, a decrease of three orders of magnitude. With this simple method, MMT-PI composite film with noticeably improved water vapor and oxygen barrier properties can be achieved, which will provide a feasible strategy for the preparation of flexible high gas barrier films.

**TABLE 1** The WVTR, OTR, and LOI of the DABPPI and MMT-PI

Sample	WVTR (g/m <sup>2</sup> /day, 77%RH)	OTR (cm <sup>3</sup> /m <sup>2</sup> /day/0.1MPa)	LOI (%)
DABPPI	2.25	1944.69	40.9
MMT-PI	0.0185	7.98	67.9

Limiting oxygen index (LOI) is one of the important indicators to characterize the combustion performance of polymers. LOI refers to the volume fraction concentration of oxygen in a mixture of oxygen and nitrogen when it is just able to support its combustion. In general, polymers with LOI greater than 27% can be considered flame retardant polymers.<sup>[43]</sup> The results (**Table 1**) show that DABPPI has an LOI of 40.9% and is a good flame retardant polymer. MMT-PI has an even higher LOI of 67.9%. It can be observed that the addition of MMT exhibits better performance on the flame retardant behavior of the developed bioinspired composites. Together, MMT and PI built a “wall” in the composite, preventing gas from entering and exiting. This “wall” had a good oxygen barrier, making it difficult for combustion-supporting gas to enter the interior of the material. Likewise, the combustible gas thermally decomposed inside was hard to release to the outside to maintain combustion. Benefiting from the strong interaction between MMT and PI, the composite presented a nearly perfect “brick-and-mortar” structure, and the LOI was greatly improved.

DABPPI burned quickly after being ignited in the LOI test, and its film frame burned out after the test (**Fig. S3** in Supporting Information). Whereas, after combustion, MMT-PI still retained its basic framework due to its good flame retardancy. This means that if it is applied in fireproof coatings, like exterior wall coatings, it may further delay the damage to the wall, thus giving people more time to escape.

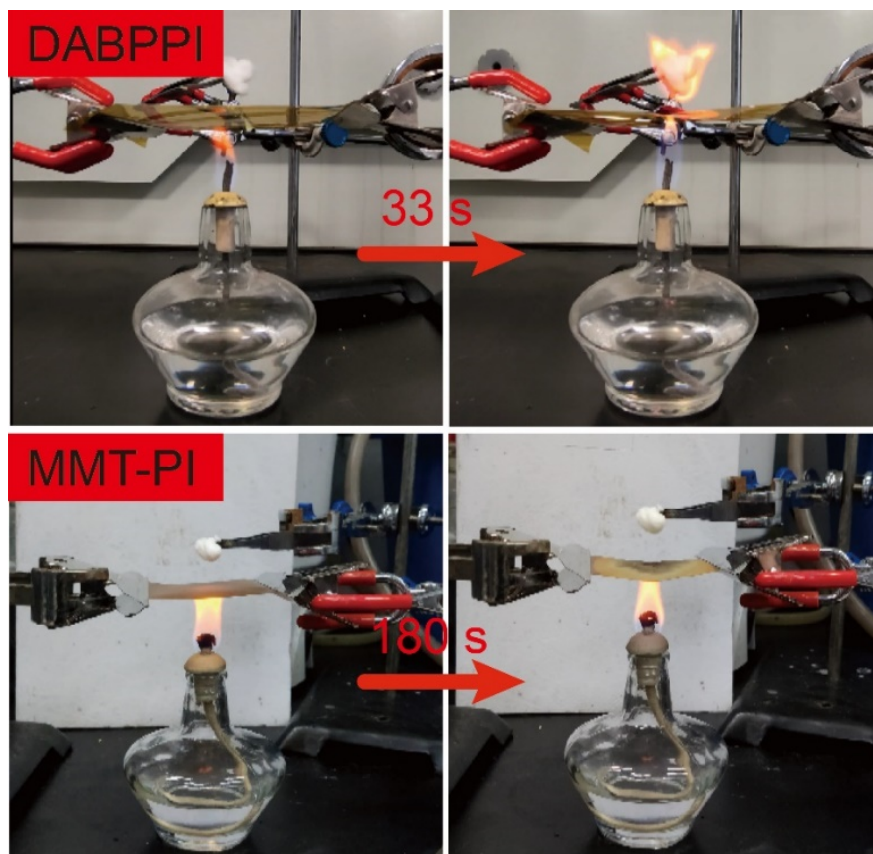


**FIGURE 3** Flame retardant tests of DABPPI and MMT-PI, both of which acted as fire shields to protect cotton.

Furthermore, to observe the flame retardancy of the composite more intuitively and comprehensively, and to explore its real application potential, MMT-PI was directly exposed to the flame of an alcohol lamp ( $600\text{ }^{\circ}\text{C}\sim 800\text{ }^{\circ}\text{C}$ ), and a fluffy cotton ball was placed above the composite (the cotton ball was about 2 cm away from MMT-PI, to check whether it will be ignited). Similarly, DABPPI was also tested as a fireproof board. Once DABPPI was exposed to flame, it would burn through after 33 s, then ignite the cotton ball. Differently, even if the MMT-PI was exposed to the flame for 180 s, it would not burn through, and the cotton ball would not catch fire (**Fig. 3**).

An infrared camera was used to record the above process (the recording time was 90 s), and the results were shown in **Fig.4** (the DABPPI results were given in **Fig. S4** in Supporting Information).

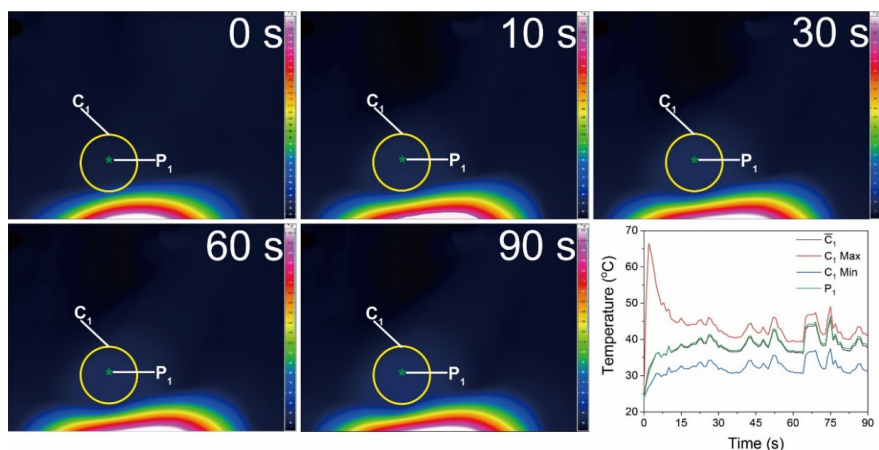


**FIGURE 4** Pseudocolor thermal images of the front view of the MMT-PI subjected to the alcohol lamp flame at different times (0 s~90 s). Time dependence of the center of the cotton ball temperature (last one).

The cotton ball was selected as the observation object, where  $C_1$  is the periphery and  $P_1$  is the center of the cotton ball, respectively. The maximum temperature of  $C_1$  was detected to be close to 70 °C when the alcohol lamp was once lit. This may be due to the small thickness of MMT-PI and the short longitudinal distance of heat transfer, which makes it easier to reach the high temperature of the MMT-PI mentioned above. Later, the temperature gradually decreased, probably due to the increased heat conduction along the plane direction. Therefore, the temperature of  $C_1$  dropped to about 45°C, subsequently kept at a constant value of no more than 50 °C. During the recorded 90 s, the cotton ball was not ignited. On the contrary, both  $C_1$  and  $P_1$  reached the maximum temperature after contact with the flame for 33 s for DABPPI (**Fig. S4** in Supporting Information), and the cotton ball ignited immediately upon exposure to the flame and burned off in 9 s.

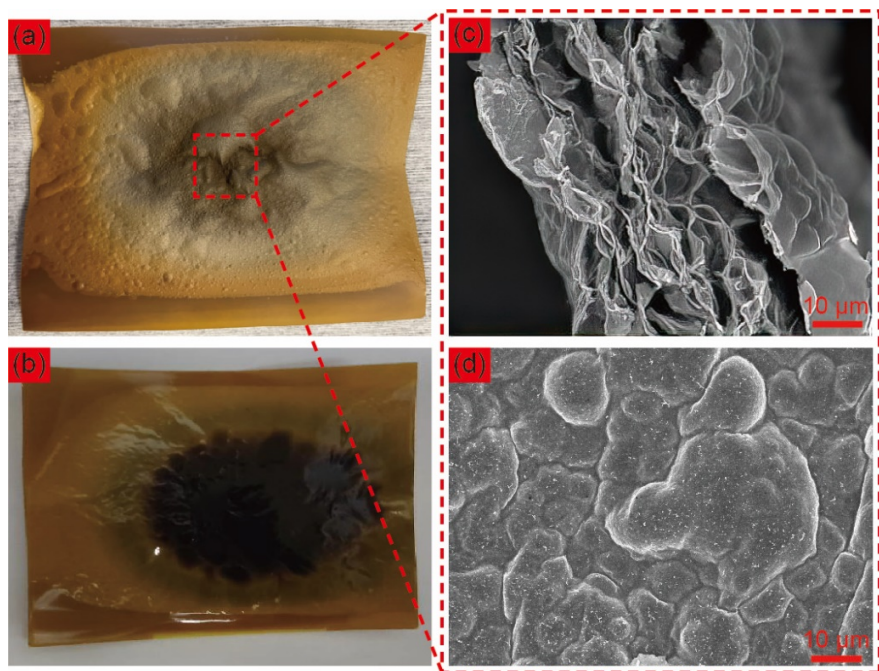


**FIGURE 5** Digital photos of MMT-PI after combustion test, (a) is composite side and (b) is substrate DABPPI side. SEM diagram of (c) cross-section and (d) surface of MMT-PI after combustion.

The flame retardancy mechanism of MMT-PI can be inferred by SEM images before and after combustion (**Fig. 5** and **Fig. S5** in Supporting Information). The layered structure of MMT-PI remained intact after burning, but the thickness increased by about 30  $\mu\text{m}$  (the thickness before combustion was about 45  $\mu\text{m}$  (**Fig. S5**)) (**Fig. 5c**). This could be attributed to the following reasons. MMT is a solid acid catalyst that can rapidly carbonize PI.<sup>[44]</sup> The carbonized products were attached to MMT, which promotes the higher gas barrier properties of the composite surface. Thereby, combustible gas released by thermal decomposition inside composites was more difficult to escape, resulting in internal expansion and the formation of many bubbles on the surface (**Fig. 5a, d**).<sup>[45]</sup> The combustible substances inside the composite were laborious in contact with oxygen, and the internal oxygen concentration was diluted and reduced, thereby enhancing the flame retardancy of MMT-PI.

In addition, the use of PI as the polymer matrix endows the bionic composite with relatively low WA% (see Supporting Information for details). In contrast, other commonly used polymer matrices for the preparation of bionic composites (such as PVA, CMC, etc.) have high water absorption or can be completely dispersed in water. Low water absorption is beneficial, when applied to fireproof exterior walls, having low water absorption will have less damage on snowy and rainy days.

Surprisingly, MMT-PAAS without thermal imidization also has fairly good flame retardant properties. We prepared MMT-PAAS bioinspired coating on a combustible PU foam. The combustion of PU foam and coating is then tested. PU foam burned out completely when it exploded into the fire (remove the ignition source as soon as the PU foam was ignited) (**Fig. 6a, b**). However, for MMT/PAAS-PU, under the same conditions, only the surface exposed to the flame was charred and then self-extinguished, and the rest remained in its original shape (**Fig. 6c, d**). After combustion, the MMT-PAAS expanded in the coating layer of MMT/PAAS-PU, but its layered structure was preserved (**Fig. 6e, f**). This loose lamellar structure effectively isolated external oxygen and heat,<sup>[46]</sup> so that the wrapped PU will not be ignited, showing excellent flame retardant performance.

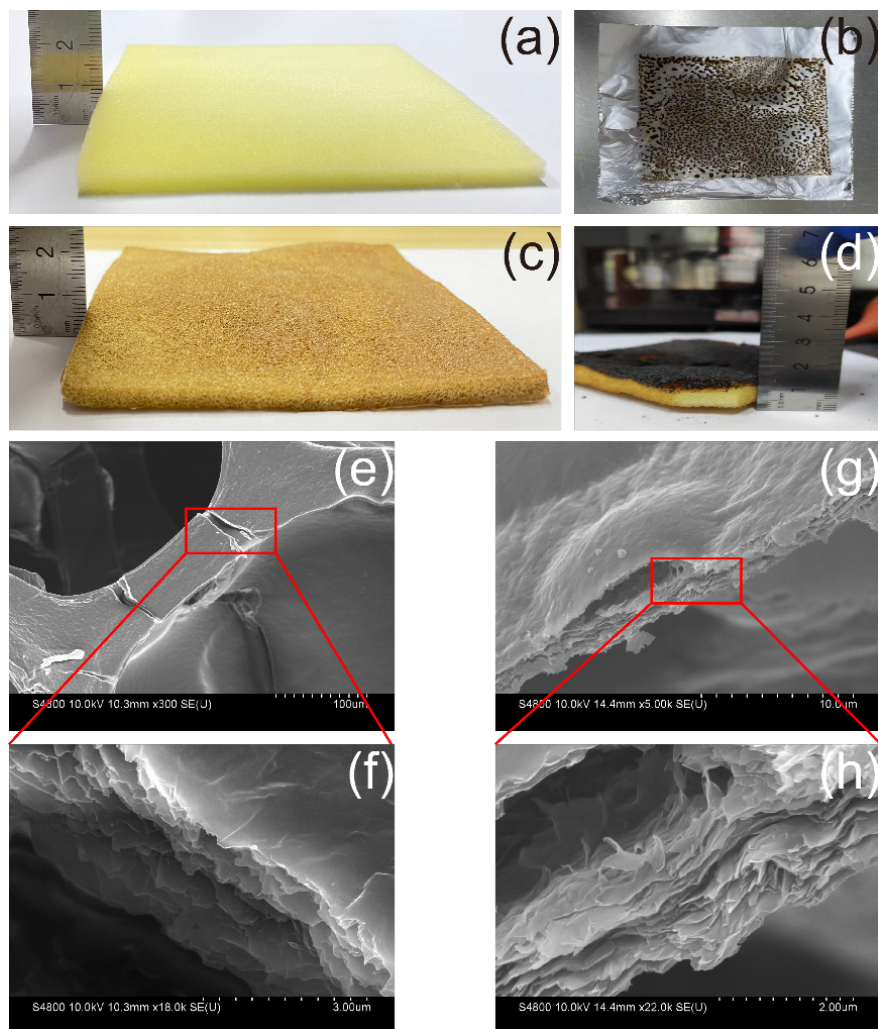


**FIGURE 6** Digital photos of PU foam (a, b) and MMT/PAAS-PU (c, d) before and after burring. SEM images of MMT/PAAS-PU before (e, f) and after (g, h) burring.

Subsequently, the effect of MMT/PAAS coating on the flame retardancy of PU foam was studied by using a cone calorimetric test (CCT). The results are shown in **Fig.7** and the characteristic parameters are shown in **Table 2**. The most obvious should be shown to slow its ignition time. The time to ignition (TTI) of PU foam is 6s, while that of MMT/PAAS-PU is 10s. After the material was ignited, the heat release rate (HRR) of PU foam was almost higher than that of the MMT/PAAS-PU throughout the test (**Fig. 7a**). Especially, its peak HRR (PHRR) was  $381.42 \text{ kW/m}^3$ , 53.39% higher than that of MMT/PAAS-PU ( $177.80 \text{ kW/m}^3$ ). Furthermore, the total heat release (THR) of PU foam is 40.69% larger (**Fig.7b**). Unlike completely burned-out PU foam, MMT/PAAS-PU self-extinguished during the test (**Fig. S7** in Supporting Information). Based on the above results, the MMT/PAAS coating will effectively improve the flame retardant properties and reduce damage even after ignition. Relatively, the peak mass loss rate (PMLR) is also higher than that of MMT/PAAS-PU, indicating that under a certain fire intensity, the degree of pyrolysis, volatilization, and combustion is more intense. Since the MMT/PAAS coating has an ordered layered structure and the structure remains after combustion, it plays a good role in the gas barriers. Therefore, compared with PU foam, its peak effective heat combustion (PEHC, reflecting the combustion degree of volatile gas in gas phase flame), total smoke production (TSP), peak CO yield (PCOY) and peak

CO<sub>2</sub> yield (PCO<sub>2</sub>Y) decreased by 15.76%, 53.03%, 47.58%, and 70.15%, respectively. The smoke produce rate (SPR) is always lower than PU foam (**Fig.7c**) during the whole test. In a real fire, more than half of the deaths are caused by particulate matter and toxic gases (especially CO) generated by combustion.<sup>[47]</sup> MMT/PAAS coating in this study can effectively suppress smoke, which may greatly save people’s lives in real fires.

**TABLE 2** The resulting parameters of CCT for PU foam and MMT/PAAS-PU

Sample	PHRR (kW/m <sup>3</sup> )	PMLR (g/s)	PEHC (MJ/kg)	THR (MJ/m <sup>3</sup> )	TSP (m <sup>3</sup> )	PCOY (kg/kg)	PCO <sub>2</sub> Y (kg/kg)
PU foam	381.42	0.122	53.56	16.08	1.69	11.35	171.89
MMT/PAAS-PU	177.80	0.077	45.12	9.54	0.79	5.95	51.31

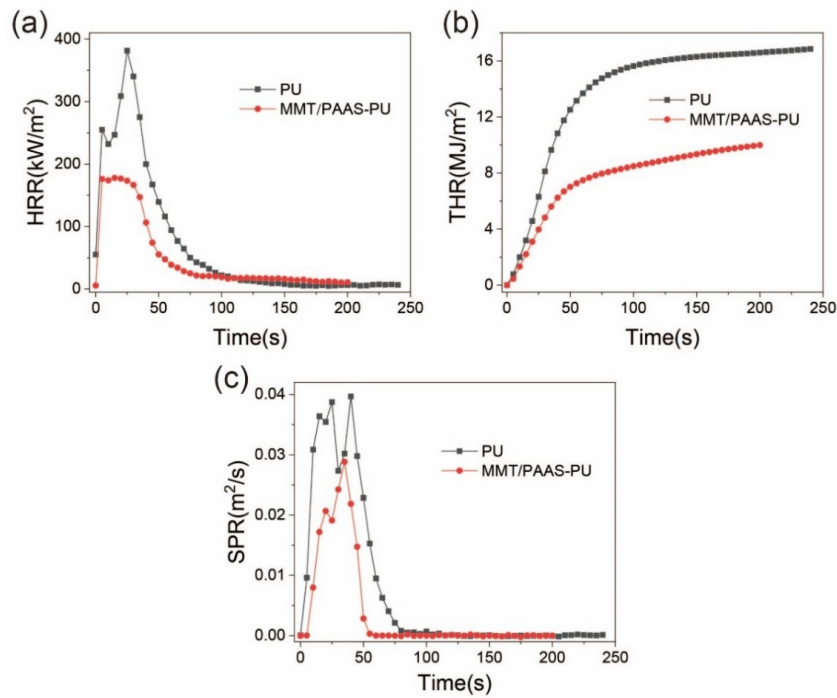


**FIGURE 7** The (a) HRR, (b) THR, and (c) SPR data of PU foam and MMT/PAAS-PU.

#### 4. Conclusion

We successfully fabricated biomimetic composites with layered “brick-and-mortar” structures using polyimide and MMT through a gravity-induced deposition. This layered structure can effectively block the entry of gases and hinder their diffusion. The WVTR of the composite decreased by 99.18% to 0.0185 g/m<sup>2</sup>/day and its OTR dropped by three orders of magnitude to 7.98 cm<sup>3</sup>/m<sup>2</sup>/day/0.1MPa. Furthermore, this structure can prevent the escape of internal combustible gas, which enables the composite to have excellent flame retardant properties, and the LOI is increased from 47.9% to 67.9%. Benefiting from the low hygroscopicity of polyimide, MMT-PI has better control of water absorption compared to common biomimetic composites. In addition to being used alone as a self-supporting film, it also exhibits excellent flame retardancy when used as a coating. After the PU foam was simply immersed into MMT-PAAS glue and dried from the

solvents, the MMT/PAAS-PU had self-extinguishing properties. Its PHRR, THR, and TSP decreased by 53.39%, 40.69%, and 53.03% respectively. This work confirms that the layered structure is effective for the improvement of flame retardancy and expands the polymer family used in the preparation of biomimetic composites. Furthermore, our work provides a simple strategy for the preparation of biomimetic composites with low water absorption, high gas barrier properties, and good flame retardancy, with great application potential in numerous fields.

## Notes

The authors declare no conflict of interest.

## Acknowledgment

The authors gratefully acknowledge the financial support of the projects from Ministry of Science and Technology (No. 2022YFB3806601), National Natural Science Foundation of China (Nos. U20A20255, 51873239, 52103022, and 52203286), Guangdong Provincial Department of Science and Technology (2020B010182001, 2020B010179001, 2021A1515010664, and 2019B040401002), and Fellowship of China Postdoctoral Science Foundation (No. 2022M723572).

## References

1. P. Tran, Q. T. Nguyen, K. Lau, *Composites Part B: Engineering* ,**2018** , 155, 31-48.
2. Z. K. Brzozowski, D. Kijeńska, W. Zatorski, *Designed Monomers and Polymers* , **2002** , 5, 183-193.
3. Y. Zhang, J. He, R. Yang, *Polymer Degradation and Stability* ,**2016** , 125, 140-147.
4. Z. Wang, X. Shen, Y. Yan, T. Qian, J. Wang, Q. Sun, C. Jin, *Applied Surface Science* , **2018** , 450, 387-395.
5. C. Wang, Y. Wu, Y. Li, Q. Shao, X. Yan, C. Han, Z. Wang, Z. Liu, Z. Guo, *Polymers for Advanced Technologies* , **2018** , 29, 668-676.
6. H. Liu, M. Dong, W. Huang, J. Gao, K. Dai, J. Guo, G. Zheng, C. Liu, C. Shen, Z. Guo, *Journal of Materials Chemistry C* , **2017** , 5, 73-83.
7. X. Qiu, Z. Li, X. Li, Z. Zhang, *Chemical Engineering Journal* ,**2018** , 334, 108-122.
8. J. H. Yang, W. Zhang, H. Ryu, J. H. Lee, D. H. Park, J. Y. Choi, A. Vinu, A. A. Elzatahry, J. H. Choy, *Journal of Materials Chemistry A* , **2015** , 3, 22730-22738.
9. Y. Zhang, W. Cheng, W. Tian, J. Lu, L. Song, K. M. Liew, B. Wang, Y. Hu, *ACS Applied Materials & Interfaces* , **2020** , 12, 6371-6382.
10. Z. R. Yu, M. Mao, S. N. Li, Q. Q. Xia, C. F. Cao, L. Zhao, G. D. Zhang, Z. J. Zheng, J. F. Gao, L. C. Tang, *Chemical Engineering Journal* , **2021** , 405, 126620.
11. L. Yin, K. Gong, K. Zhou, X. Qian, C. Shi, Z. Gui, L. Qian, *Journal of Colloid and Interface Science* , **2022** , 608, 853-863.
12. J. Zhu, M. U. Fawn, B. M. Alexander, A. W. Charles, *Chemistry of Materials* , **2001** , 13, 4649-4654.
13. F. Song, A. K. Soh, Y. L. Bai, *Biomaterials* , **2003** , 24, 3623-3631.
14. H. L. Gao, Z. Y. Wang, C. Cui, J. Z. Bao, Y. B. Zhu, J. Xia, S. M. Wen, H. A. Wu, S. H. Yu, *Advanced Materials* , **2021** , 33, 2102724.
15. S. Wan, X. Li, Y. Chen, N. Liu, Y. Du, S. Dou, L. Jiang, Q. Cheng, *Science* , **2021** , 374, 96-99.
16. Q. Yu, L. Zhu, T. Liu, S. S. Babu, Z. Zheng, S. Liu, Z. Cui, Y. Zhang, J. Xu, *Advanced Materials Interfaces* , **2021** , 8, 2001786.

17. Z. Chen, W. Chen, P. Liu, Y. Liu, Z. Liu, *Composites Part A: Applied Science and Manufacturing* , **2021** , 150, 106598.
18. D. Jiao, J. Zhang, Y. Y. Liu, X. G. Liu, Q. Zhang, S. F. Tang, Z. Q. Liu, Z. F. Zhang, *Carbon* , **2021** , 171, 409-416.
19. H. Zhao, J. Ding, P. Liu, H. Yu, *Corrosion Science* ,**2021** , 183, 109333.
20. H. Li, C. Teng, J. Zhao, J. Wang, *Composites Science and Technology* , **2021** , 201, 108543.
21. W. Liu, R. Li, J. Liu, X. Ma, Y. Xiao, Y. Wang, *Carbon* ,**2021** , 184, 618-626.
22. W. Xin, C. Lin, L. Fu, X. Y. Kong, L. Yang, Y. Qian, C. Zhu, Q. Zhang, L. Jiang, L. Wen, *Matter* , **2021** , 4, 737-754.
23. H. Xie, X. Lai, H. Li, J. Gao, X. Zeng, X. Huang, X. Lin, *Chemical Engineering Journal* , **2019** , 369, 8-17.
24. Z. Wang, M. Hu, X. Yu, H. Li, Q. Wang, L. Li, *Journal of Membrane Science* , **2021** , 637, 119622.
25. H. Zeng, J. Wu, H. Pei, Y. Zhang, Y. Ye, Y. Liao, X. Xie, *Chemical Engineering Journal* , **2021** , 405, 126865.
26. S. Song, C. Zhang, J. Wang, W. Li, Z. Jiang, Y. Zhang, *Sensors and Actuators B: Chemical* , **2021** , 332, 129446.
27. X. Liu, Y. Song, Q. Xu, Q. Luo, Y. Tian, C. Dang, H. Wang, M. Chen, Y. XXuan, Y. Li, Y. Ding, *Solar Energy Materials and Solar Cells* ,**2021** , 230, 111240.
28. W. Prins, J. Hermans, *Journal of Physical Chemistry* ,**1959** , 63, 716-720.
29. Y. Tao, C. Huang, C. Lai, C. Huang, Q. Yong, *Carbohydrate Polymers* , **2020** , 245, 116508.
30. D. J. Liaw, K. L. Wang, Y. C. Huang, K. R. Lee, J. Y. Lai, C. S. Ha, *Progress in Polymer Science* , **2012** , 37, 907-974.
31. H. J. Ni, J. G. Liu, Z. H. Wang, S. Y. Yang, *Journal of Industrial & Engineering Chemistry* , **2015** , 28, 16-27.
32. T. Sekitani, U. Zschieschang, H. Klauk, T. Someya, *Nature Materials* , **2010** , 9, 1015-1022.
33. Y. Ding, B. Bikson, J. K. Nelson, *Macromolecules* ,**2002** , 35, 905-911.
34. A. Karimi, W. M. A. W. Daud, *Polymer Composites* ,**2017** , 38, 1086-1102.
35. S. Li, S. Wang, X. Du, H. Wang, X. Cheng, Z. Du, *Progress in Organic Coatings* , **2021** , 106613.
36. D. H. Lee, Y. Bae, Y. N. Kim, J. Y. Sung, S. W. Han, D. P. Kang, *Langmuir* , **2018** , 34, 219-227.
37. A. K. Saini, C. M. Carlin, H. H. Patterson, *Journal of Polymer Science Part A: Polymer Chemistry* , **1992** , 30, 419-427.
38. K. Zhang, Q. Yu, L. Zhu, S. Liu, Z. Chi, X. Chen, Y. Zhang, J. Xu, *Polymers* , **2017** , 9, 677.
39. Y. Chen, H. Liu, L. Yu, Q. Duan, Z. Ji, L. Chen, *ACS Sustainable Chemistry & Engineering* , **2020** , 8, 10423-10430.
40. C. Huang, G. Fang, Y. Tao, X. Meng, Y. Lin, S. Bhagia, X. Wu, Q. Yong, A. J. Ragauskas, *Carbohydrate Polymers* , **2019** , 225, 115219.
41. E. S. Tsurko, P. Feicht, C. Habel, T. Schilling, M. Daab, S. Rosenfeldt, J. Breu, *Journal of Membrane Science* , **2017** , 540, 212-218.
42. A. Eckert, T. Rudolph, J. Guo, T. Mang, A. Waltherr, *Advanced Materials* , **2018** , 30, 1802477.

43. X. Yang, A. Shen, Y. Jiang, Y. Meng, H. Wu, *Construction and Building Materials* , **2021** , 302, 124148.
44. R. Song, Z. Jiang, W. Bi, W. Cheng, J. Lu, B. Huang, T. Tang, *Chemistry-A European Journal* , **2007** , 13, 3234-3240.
45. H. Xie, X. Lai, Y. Wang, H. Li, X. Zeng, *Journal of Hazardous Materials* , **2019** , 365, 125-136.
46. H. Xie, X. Lai, H. Li, J. Gao, X. Zeng, X. Huang, S. Zhang, *Chemical Engineering Journal* , **2020** , 382, 122929.
47. P. Carty, S. White, *Polymer degradation and stability* **2002** , 75, 173-184.

## Graphic for manuscript

### Bioinspired polyimide film with fire retardant and gas barrier properties by gravity-induced deposition of montmorillonite

Qiao-Xi Yu, Run-Xin Bei, Jia-Hui Liu, Yan-Wei He, Si-Wei Liu\*, Zhen-Guo Chi, Jia-Rui Xu, and Yi Zhang\*

